Journal of Polymer Research (2020) 27: 375
https://doi.org/10.1007/s10965-020-02343-7

ORIGINAL PAPER

# Preparation of melamine–formaldehyde resin-microencapsulated ammonium polyphosphate and its application in flame retardant rigid polyurethane foam composites

Gang Tang[1,2,3,4] · Haohao Jiang[1] · Yadong Yang[1] · Depeng Chen[1] · Chunlin Liu[1] · Ping Zhang[2] · Lin Zhou[2] · Xinjie Huang[1] · Hao Zhang[1] · Xiuyu Liu[1,3]

Received: 12 May 2020 / Accepted: 3 November 2020 / Published online: 19 November 2020


## Abstract

Melamine–formaldehyde resin-microencapsulated ammonium polyphosphate (MFAPP) was prepared by in situ polymerization using melamine–formaldehyde (MF) resin as the shell material. MFAPP was characterized by X-ray photoelectron spectroscopy (XPS), Fourier transform infrared spectroscopy (FTIR), thermogravimetric analysis (TGA), and scanning electron microscopy (SEM), which confirmed its successful fabrication. MFAPP was further introduced to prepare rigid polyurethane foam/microencapsulated ammonium polyphosphate composites (RPUF/MFAPP). The flame retardancy, water resistance, physical properties, and thermal stability of RPUF/MFAPP were compared with virgin RPUF and RPUF/APP composite. RPUF/MFAPP30 possessed excellent flame retardancy. Even after immersion in water for 15 days, RPUF/MFAPP30 achieved V-1 rating in UL-94 test with limiting oxygen index (LOI) of 21.3 vol%, which was better than that of RPUF/APP30 with equivalent APP loading. The compressive strength of RPUF/MFAPP30 was 0.295 MPa, which was 13.5% higher than that of RPUF/APP30. Thermogravimetric analysis-Fourier transform infrared spectroscopy (TGA-FTIR) was applied to investigate gaseous products of the decomposition process for RPUF/APP and RPUF/MFAPP. It was found that the intensities of $CO_2$, isocyanate compounds, and CO for RPUF/MFAPP were lower than the values for RPUF/APP, indicating superior fire safety of RPUF/MFAPP. SEM and Raman spectra confirmed that RPUF/MFAPP30 possessed more compact char residue with higher thermal resistance, which was thus better able to inhibit mass and heat transmission in combustion. Consequently, a possible gas–solid flame-retardant mechanism of the RPUF/MFAPP composite was proposed.

**Keywords** Rigid polyurethane foam · Composites · Ammonium polyphosphate · Microencapsulation · Flame retardant

## Introduction

Rigid polyurethane foam (RPUF) is a novel porous material fabricated by reaction of polyols and isocyanates. Because of its excellent insulation performance, low cost, and corrosion resistance properties, RPUF is widely applied in applications such as building insulation, refrigeration, the petrochemical industry, and home decoration [1–7]. However, RPUF is rich in carbon and hydrogen, with a porous structure, making it easily combustible; this shortcoming limits its further application in related fields [8, 9]. Therefore, the development of methods to improve the flame-retardant performance of RPUF composites is important.

Generally, reactive and additive flame-retardant strategies have been the most common methods used to enhance the fire performance of RPUF composites [10]. Recently, a novel surface flame-retardant technique was proposed by

✉ Depeng Chen
dpchen@ahut.edu.cn

1 School of Architecture and Civil Engineering, Anhui University of Technology, 59 Hudong Road, Ma'anshan, Anhui 243002, China

2 State Key Laboratory of Environment-Friendly Energy Materials &, School of Materials Science and Engineering, Southwest University of Science and Technology, Mianyang 621010, Sichuan, China

3 Nanjing Gongda Kaiyuan Environmental Protection Technology (Chuzhou) Co., Ltd, Chuzhou 239000, Anhui, China

4 ASAP Technology (Jiangxi) Co, Ltd, Ji'an 330000, Jiangxi, China

Jiang et al., who developed a halogen-free UV-curable self-extinguishing coating, which was introduced onto the surface of RPUF to obtain a surface flame-retardant RPUF system (SFR-RPUF). SRF-RPUF demonstrated excellent fire performance with a coating thickness of 25 μm, exhibiting fast self-extinguishing behavior in fire [11]. Huang et al. incorporated 2-isocyanatoethyl methacrylate-modified MXene (m-MXene) into an intumescent flame-retardant (IFR) coating system, which was further used to prepare coated RPUF via spray-coating and UV-curing. It was observed that IFR/MXene-coated RPUF with only 1 wt% m-MXene loading possessed outstanding fire retardancy, with fast self-extinguishing, and maintained the initial shape after burning [12]. These flame-retardant strategies for RPUF and RPUF composites mainly used additives. Among the additive flame retardants, ammonium polyphosphate (APP) has the advantages of low cost and high flame efficiency, and is widely used in wood, rubber, and plastic products [13]. Wang et al. [14] combined APP with aluminum hydroxide (ATH) to improve the flame retardancy of wood-flour/polypropylene composites (WPC). It was found that when the mass ratio of APP/ATH was 2:1, WPC demonstrated the lowest total heat release with the highest graphitization. Yin et al. [15] combined APP with PER to form an IFR system and investigated the effect of the mass ratio of APP/PER on the fire performance of the PP composites. When the mass ratio of APP/PER was 2:1, the PP composites showed a limiting oxygen index (LOI) of 32.8 vol%, with a V-0 rating in the UL-94 test.

However, APP has poor compatibility with the polymer matrix, poor water resistance, and is susceptible to moisture, which causes APP particles to easily migrate to the surface of the material, especially in high-temperature and humid environments, resulting in deterioration of the mechanical properties and flame retardancy of the material [16].

Microencapsulation is a novel technology which uses natural or synthetic polymer to encapsulate solid or liquid in capsules with diameters of 1–1000 μm, generating a core–shell structure which can effectively improve the environmental resistance of the composites by forming a new interface on the surface of the core particles [17–19]. Shen et al. [20] prepared 4-oxydiphenylamine-formaldehyde (OF) resin-microencapsulated APP (OFAPP) and applied it to polyurethane composites to enhance their flame retardancy. The OFAPP exhibited improved hydrophobicity, and PU composites with OFAPP loading showed better flame retardancy compared with their counterparts with equivalent APP addition. Li et al. [21] fabricated polymethyl methacrylate-microencapsulated APP (PMAPP) and further investigated the flame retardancy and mechanical properties of RPUF/PMAPP composites. It was confirmed that PMAPP exhibited reduced hygroscopicity, and RPUF/PMAPP composites with 25% PMAPP loading demonstrated an LOI value of 25.3 vol%, and also showed higher compressive strength than that of the RPUF/APP composite. Zheng et al. [22] prepared microencapsulated ammonium polyphosphate (MAPP) by in situ polymerization of melamine (MEL) with diphenyl methane diisocyanate (MDI). MAPP was combined with expandable graphite (EG) to fabricate flame-retardant PU rigid foam composites. It was confirmed that the hydrophobicity and thermal stability of MAPP were significantly improved. PU rigid foam composites showed greatly enhanced flame retardancy, which was attributable to the synergistic effect between MAPP and EG.

Melamine–formaldehyde resin is often used as shell material for flame-retardant particles, and can significantly improve the compatibility of the flame-retardant particles with the polymer matrix, effectively inhibiting the migration of flame-retardant particles and improving the flame retardancy of the composites. Wu et al. [23] encapsulated APP with urea-melamine–formaldehyde (UMF) and applied it to polypropylene (PP). The results showed that microencapsulation significantly reduced the water solubility of APP, and the PP/MCU-APP composite demonstrated a higher LOI value than the PP/APP composite. Wu et al. [24] prepared melamine–formaldehyde resin (MF)-microencapsulated aluminum hypophosphite (MFAHP) and applied it to ABS composites. It was confirmed that MF resin enhanced the water resistance of AHP, and the addition of MFAHP effectively improved the mechanical properties of the ABS/MFAHP composites. In addition, a significant reduction was observed in the heat release rate (HRR), total heat release (THR), and total smoke production (TSR) of the ABS/MFAHP composites. Zhu et al. [25] prepared MF resin-microencapsulated double hydroxides (MCLDHs) and introduced them into epoxy resin (EP). The results showed that the contact angle of the MCLDHs was increased to 122.1° versus 8.9° with virgin LDH. In addition, the EP/ MCLDH composites presented a UL-94 V-0 rating with 30 wt% MCLDH loading.

However, there are few reports about the application of melamine–formaldehyde resin-microencapsulated ammonium polyphosphate in rigid polyurethane foam. This work aimed to fabricate microencapsulated ammonium polyphosphate (MFAPP) using melamine–formaldehyde resin as the shell material. The MFAPP was then applied to fabricate a RPUF/MFAPP composite. Thermal conductivity, thermal stability, flame retardancy, and water resistance were investigated using a thermal conductivity meter, thermal gravimetric analysis (TGA), limiting oxygen index (LOI), UL-94 vertical burn test, and scanning electron microscopy (SEM). The gaseous products of the composites were characterized by TGA-FTIR. The char residue of the composites was investigated by Raman spectra and scanning electron microscopy (SEM). Consequently, based on the results, a possible gas–solid flame-retardant mechanism was proposed for the RPUF/MFAPP composite.

## Experimental

### Materials

Polyether polyol (LY-4110, viscosity: 2500 mPa·s, hydroxyl number: 430 mg KOH/g), triethylenediamine (A33, 33%), and silicone surfactant (AK8805) were kindly provided by Jiangsu Luyuan New Materials Co., Ltd, China. Polymethylene polyphenyl polyisocyanate (PAPI) was provided by Wanhua Chemical Group Co., Ltd, China. Silicone oil foam stabilizer (AK8805) was provided by Jining Hengtai Chemical Co., LTD, China. Dibutyltin dilaurate (LC) was purchased from Air Products and Chemicals, Inc. Melamine (MEL), formaldehyde, triethanolamine (TEOA), sodium carbonate, hydrochloric acid, and ethanol were purchased from Sinopharm Chemical Reagent Co., Ltd, China. Ammonium polyphosphate (APP, polymerization degree $n > 1000$) was purchased from Jinan Fine Chemical Co., LTD, China. Distilled water was made in our laboratory.

### Preparation of MFAPP

10 g melamine, 17.9 ml formaldehyde, and 50 ml distilled water were added to a 500 ml three-neck flask with a mechanical stirrer, and the pH of the solution was adjusted to 8–9 by 10 wt% $Na_2CO_3$ solution. The temperature of the solution was increased to 80 °C and held for 30 min to obtain a transparent melamine–formaldehyde aqueous prepolymer solution.

60 g APP, 150 ml ethanol, and the melamine–formaldehyde aqueous prepolymer solution were put into a 500 ml three-neck flask with a mechanical stirrer. The pH value of the mixture was adjusted to 3–4 by 5wt% HCl solution. The mixture was then heated to 80 °C and held for 2 h. After that, the mixture was cooled to room temperature, filtered, washed with ethanol three times, and dried at 80 °C for 8 h to obtain MFAPP powder.

### Preparation of RPUF composites

The RPUF composites were prepared by a one-step water-blown method, and the formulation of the composites is listed in Table 1. LY-4110, LC, A33, AK-8005, TEA, distilled water, and flame retardants required for the experiment were added to a 500 mL beaker and mixed well with a high-speed mechanical stirrer. Then PAPI was added to the beaker with vigorous stirring for 10 s and quickly poured into a mold (300 mm × 200 mm × 60 mm). Subsequently, the foams were cured at 80 °C for 5 h to complete the polymerization process. The foams were then cut into a suitable size for further characterization.

### Measurement and characterization

Scanning electron microscopy (SEM; JSM-6490LV, JEOL Ltd., Japan) was used to investigate the morphology of the MFAPP particles, RPUF composites, and the char residues with accelerating voltage of 20 kV. In order to enhance the conductivity, the samples were coated with a thin conductive layer before observation.

X-ray photoelectron spectroscopy (XPS; VG ESCALAB MkII spectrometer, VG Co., Ltd., UK) was used to investigate the elemental content of APP and MFAPP with Al Kα excitation radiation ($h\nu = 1253.6$ eV) in ultrahigh vacuum conditions.

Thermogravimetric analysis (TGA; Q5000IR thermogravimetric analyzer, TA Instruments, USA) was used to test the thermal stability of the APP, MFAPP, and RPUF composites at a heating rate of 20 °C/min in air atmosphere. The temperature range was room temperature to 800 °C and with 5–10 mg of samples.

Fourier transform infrared spectrometry (FTIR; Nicolet 6700 FTIR spectrophotometer) was used to characterize APP and MFAPP using a KBr disk. The transition mode was used and the wavenumber range was set from 4000 to 400 $cm^{-1}$.

For the water resistance test, the samples were immersed in water at room temperature (25 °C) for 5, 10, and 15 days, then dried at 60 °C for 24 h to constant weight, and further characterized by LOI, UL-94, and SEM.

Thermogravimetric analysis-Fourier transform infrared spectrometry (TGA-FTIR): TGA-FTIR was performed using a Q5000IR (TA Instruments, USA) thermo-analyzer linked to a Nicolet 6700 FTIR spectrophotometer (Thermo Scientific, USA). About 5–10 mg of the sample was placed in an alumina crucible and heated from 30 to 700 °C. The heating

**Table 1** Formulation of RPUF, RPUF/APP30, and RPUF/MFAPP30

| Sample | LY-4110 php[a] | PM200 php | LC php | AK-8805 php | A33 php | TEA php | Water php | APP php | MFAPP php |
|---|---|---|---|---|---|---|---|---|---|
| RPUF | 100 | 150 | 0.5 | 2 | 1 | 3 | 2 | 0 | 0 |
| RPUF/APP30 | 100 | 150 | 0.5 | 2 | 1 | 3 | 2 | 30 | 0 |
| RPUF/MFAPP | 100 | 150 | 0.5 | 2 | 1 | 3 | 2 | 0 | 30 |

[a]parts per hundred polyol.

rate was 20 °C/min in a nitrogen atmosphere with a flow rate of 70 ml/min.

Apparent density: The apparent density of the RPUF composites was measured according to ISO 845–2006, in which the size of the sample was no less than 100 $cm^3$. Five samples were tested to obtain the average value.

Thermal conductivity: A thermal conductivity meter (TC3000E, Xiaxi Electronic Technology Co., Ltd, China) was introduced to measure thermal conductivity according to GB/T 10297–2015, with sample size of 30 mm × 30 mm × 25 mm. Five parallels for each sample were tested and the average value was reported.

Compressive strength: A universal testing machine (WSM-20 KB, China) was applied to investigate the compressive strength of the samples according to GB/T8813-2008, with sample size of 50 mm × 50 mm × 40 mm. Five parallels for each sample were tested to obtain the average value.

UL-94 vertical burn test: The vertical burn test was conducted according to ASTM D3801-96 using a CZF-3 instrument (Jiangning Analysis Instrument Co., Ltd, China) with sample dimensions of 127 mm × 13 mm × 10 mm.

Limiting oxygen index (LOI): LOI values for the samples were measured at room temperature using a JF-3 oxygen index instrument (Jiangning Analysis Instrument Co., Ltd, China) according to ASTM D2863-97, with sample dimensions of 127 mm × 10 mm × 10 mm.

Raman spectroscopy: The char residue of the samples was obtained by calcining the composites at 700 °C for 10 min. The char residue was further characterized by laser Raman spectroscopy (LRS, inVia, Renishaw, London, UK). The excitation wavelength was 514 nm with the wavenumber range set from 800 to 2000 $cm^{-1}$ and resolution of 1 $cm^{-1}$.

## Results and discussion

### Characteristics of MFAPP

Figure 1 presents the FTIR spectrum of MFAPP and APP. It can be seen that the peak at around 3200 $cm^{-1}$ corresponds to the N–H stretching vibration of APP. The peaks at around 1075 $cm^{-1}$ and 880 $cm^{-1}$ correspond to asymmetric stretching vibration and stretching vibration of the P–O bond [26], which are typical absorption peaks of APP. The peak at 1651 $cm^{-1}$ can be ascribed to the stretching vibration of the C = O bond in the –N–(CO)–N– structure [27]. The peak at 1552 $cm^{-1}$ confirms the existence of a nitrogen heterocyclic ring for melamine. The FTIR spectra of MFAPP reveal typical peaks not only for APP but also for melamine formaldehyde resin, indicating the successful fabrication of MFAPP.

X-ray photoelectron spectrometry is an effective method for characterizing the chemical composition

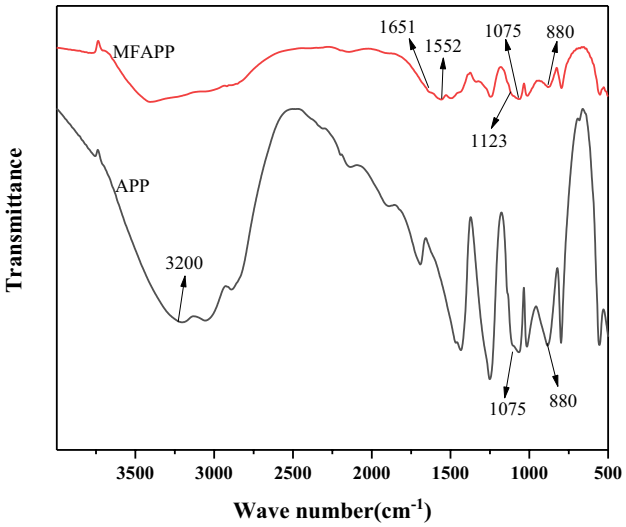


**Fig. 1** FTIR spectra of APP and MFAPP

of materials [28]. Figure 2 presents the XPS spectra of APP and MFAPP, and the corresponding data are listed in Table 2. The peaks at around 532 eV and 400 eV are ascribed to O1s and N1s peaks, respectively. The peaks at 135 eV and 192 eV correspond to $P_{2p}$ and $P_{2s}$ peaks of APP, confirming the existence of the P element. It was observed that APP contained P of 11.7 at%, C of 28.45 at%, N of 23.06 at%, and O of 36.72 at%. After microencapsulation treatment, MFAPP showed a significant decrease in P content to 2.70%. Also, the N content in MFAPP increased to 38.65 at%, which may result from the high N content in the MF shell material. The above results imply that the MF resin was encapsulated on the surface of the APP particles.

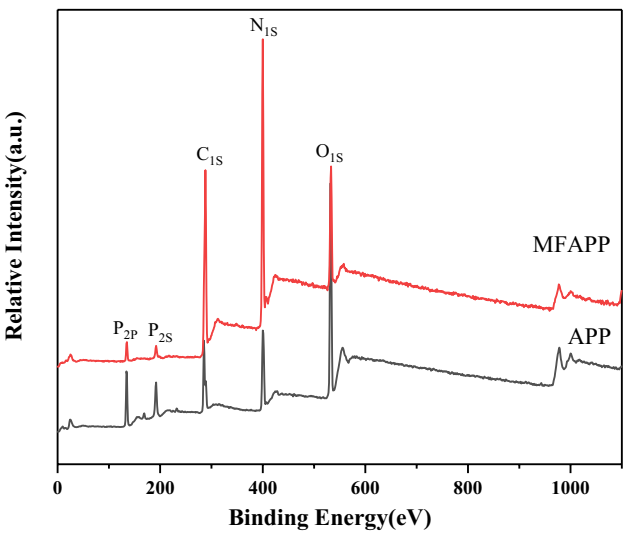


**Fig. 2** XPS spectra of APP and MFAPP

**Table 2** Elemental content of APP and MFAPP by XPS test

| Sample | P (At%) | C (At%) | N (At%) | O (At%) |
|---|---|---|---|---|
| APP | 11.77 | 28.45 | 23.06 | 36.72 |
| MFAPP | 2.70 | 46.08 | 38.65 | 12.57 |

Figure 3 presents SEM images of the APP and MFAPP particles. It can be observed that the APP particles show an irregular size with a smooth surface. After microencapsulation, MFAPP particles exhibit a rough surface, confirming the existence of the MF resin, which is consistent with the XPS test.

Figure 4 shows the TGA and derivative thermogravimetric (DTG) curves of APP and MFAPP under air conditions, and the corresponding data are presented in Table 3. As shown in the figure, the APP exhibits two decomposition stages. The initial degradation temperature ($T_{-5wt\%}$) was around 331 °C. In the first stage, APP degraded to form pyrophosphoric acid (PPA), with the release of ammonia gas and water vapor [29]. The second stage occurred mainly within the range of 500–650 °C, in which the pyrophosphoric acid produced in the previous stage further decomposed into phosphorus oxide [30]. MFAPP also exhibited two mass loss stages. The first stage occurred mainly at 251–450 °C. In this stage, MFAPP degraded into pyrophosphoric acid, releasing both $NH_3$ and $CO_2$, which promoted the formation of an intumescent char layer [31]. It can also be observed that MFAPP was more stable than APP at temperatures above 60 °C. At 700 °C, MFAPP possessed significantly enhanced char residue of 20.4 wt% compared with 10.5 wt% of APP, implying enhanced thermal stability of MFAPP.

## Thermal stability

Figure 5 presents the TGA and DTG curves for RPUF, RPUF/APP30, and RPUF/MFAPP30 composites under air conditions. RPUF began to decompose at 271 °C, with two mass loss stages. The first stage can be ascribed to the rupture of the polyurethane molecular chain, with the release of isocyanates, secondary amines, aldehydes, ketones, $CO_2$, and water. [32]. The second stage, which occurred in the range of 420–650 °C, corresponded to thermal degradation of the soft segment [33]. RPUF/APP30 presented $T_{-5\%}$ of 265 °C with two decomposition stages. It showed initial degradation stage between 220 °C and 400 °C, with $T_{max1}$ at 305 °C. The second degradation stage of RPUF/APP occurred in the range of 450–650 °C with $T_{max2}$ of 556 °C. Compared with RPUF/APP30, RPUF /MFAPP showed a significantly lower rate of mass loss and higher $T_{max1}$ value, which may be because MF resin prevented the reaction between APP and the polyurethane molecular chain. The second decomposition stage of RPUF/MFAPP was in the range of 440–650 °C. During this stage, the polyphosphoric acid generated by the thermal decomposition of APP reacted with the pyrolysis products of the matrix to promote the formation of compact char residue with excellent thermal insulation properties. Lastly, RPUF /MFAPP presented char residue of 10.1 wt% at 700 °C compared

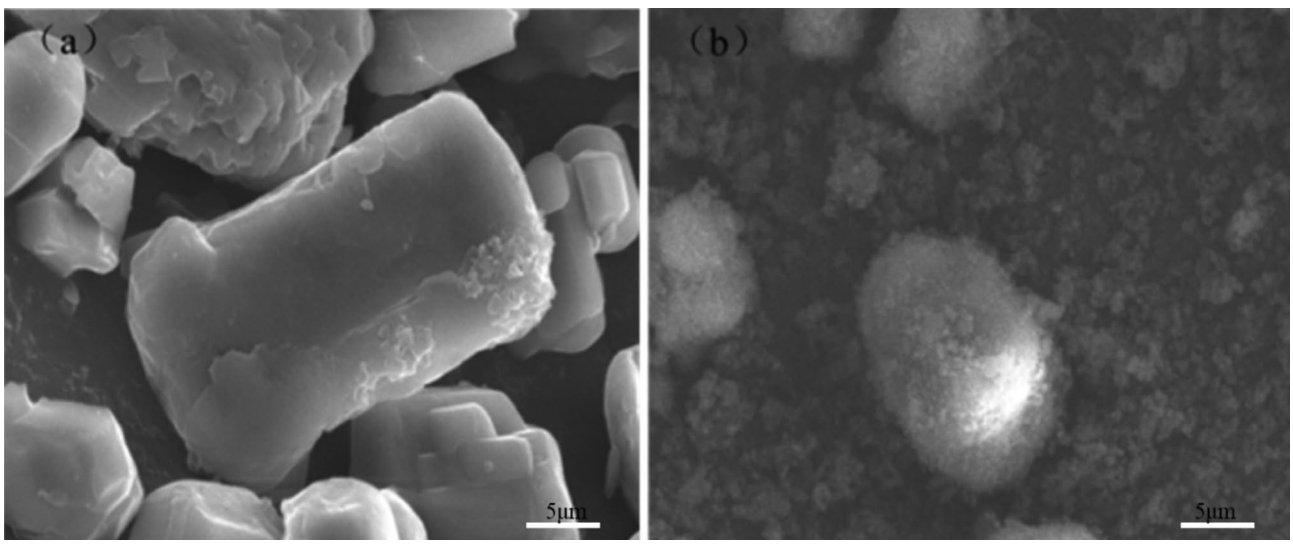


**Fig. 3** SEM images of APP (**a**) and MFAPP (**b**)

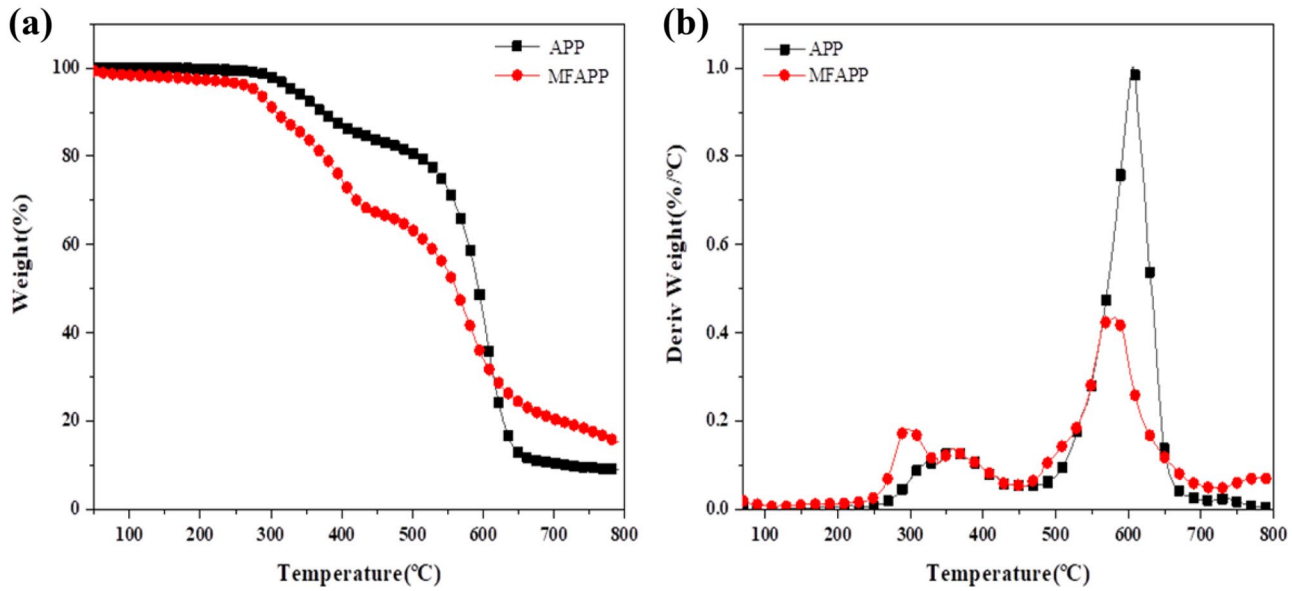


**Fig. 4** TGA (**a**) and DTG (**b**) curves of APP and MFAPP

with 1.2 wt % of virgin RPUF. It can also be seen that the TGA curves of RPUF/MFAPP30 were always greater than those of RPUF, indicating that MFAPP effectively improved the thermal stability of the RPUF composites.

## Flame-retardant properties

Figure 6 shows the test results for UL-94 and LOI of RPUF, RPUF/APP30, and RPUF/MFAPP30 composites with different immersion times. It can be seen that virgin RPUF exhibits poor flame retardancy, with LOI of 18.8 vol% and no rating in the UL-94 test. The LOI value decreased with increasing immersion time, which all failed in UL-94 test. RPUF/APP30 possessed LOI of 23.3 vol% with a V-0 rating in the UL-94 test, which also showed degraded flame retardancy with increased immersion time. RPUF/APP30 presented no rating in the UL-94 test, with a decreased LOI value of 21.7 vol% after immersion in water for 15 days. This result may reflect the poor water resistance of APP particles in RPUF/APP30. RPUF/MFAPP30 showed an LOI value of 21.3 vol%, which also passed the UL-94 test with a V-0 rating. An increase in immersion time resulted in almost no change in RPUF/MFAPP30 flame retardancy. This may be because the MF shell effectively inhibited the dissolution of APP particles, ensuring effective flame retardancy of RPUF/MFAPP30.

**Table 3** TGA data for APP, MFAPP, and RPUF composites under air conditions

| Sample | $T_{-5wt\%}$/℃ | $T_{max1}$/℃ | $T_{max2}$/℃ | Residues at 700 ℃(wt%) |
|---|---|---|---|---|
| APP | 331 | 361 | 606 | 10.5 |
| MFAPP | 277 | 297 | 578 | 20.4 |
| RPUF | 271 | 313 | 569 | 1.2 |
| RPUF/APP30 | 265 | 305 | 556 | 11.3 |
| RPUF/MFAPP30 | 259 | 321 | 567 | 10.1 |

## Morphology

Figure 7 shows the SEM images of RPUF, RPUF/APP30, and RPUF/MFAPP30 before and after the immersion test. By comparing Fig. 7 (a) and (b), it can be seen that after 15 days of immersion, partial damage appeared around the cell structure of RPUF. In Fig. 7 (c) and (d), it can be observed that some APP particles migrated to the surface of the RPUF matrix after immersion, which may have resulted from the poor compatibility between APP particles and the RPUF. It can be seen in Fig. 7(e) that RPUF/MFAPP30 composite exhibited a smooth surface. Even after immersion in water for 15 days, the surface of RPUF/MFAPP was still smooth, without precipitation of APP particles. This indicates that the organic MF resin shell effectively improved the compatibility of APP particles and RPUF matrix, which also enhanced the water resistance of APP.

## Physical properties

Table 4 displays the typical physical properties of RPUF, RPUF/APP30, and RPUF /MFAPP. RPUF showed thermal

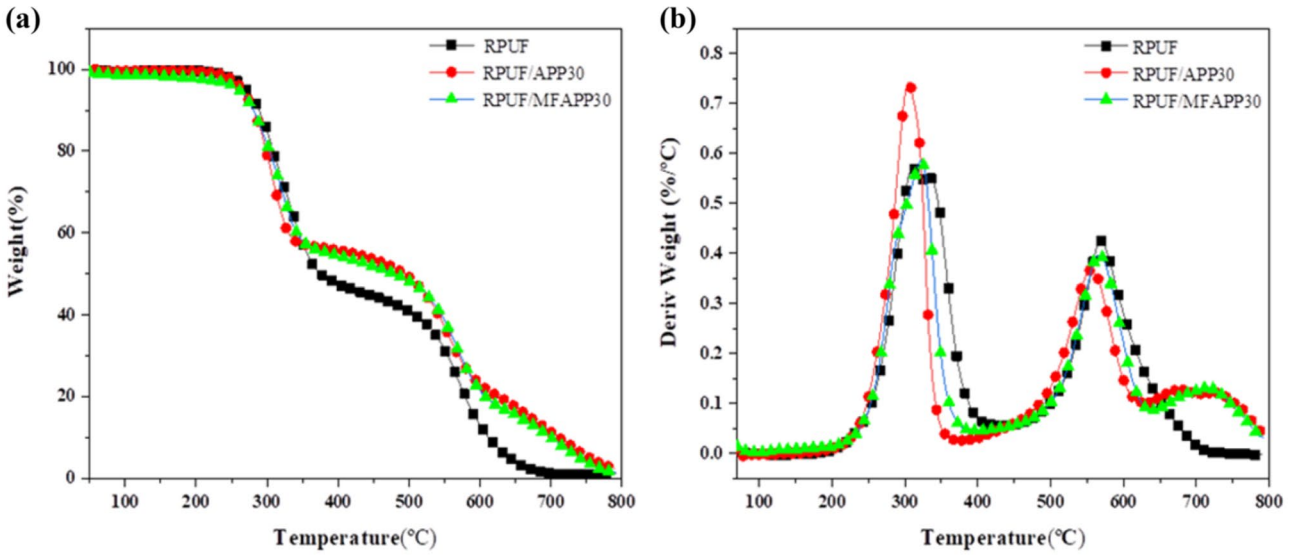


**Fig. 5** TGA (**a**) and DTG (**b**) curves of RPUF, RPUF/APP30, and RPUF/MFAPP30

conductivity of 0.0389 W/m●k, with density of 63.52 kg/m$^3$. After the addition of 30 php APP, the density of RPUF/APP30 increased to 64.16 kg/m$^3$, likely because of the higher density of the APP particles compared with the RPUF matrix. The thermal conductivity of RPUF/APP30 increased to 0.0412 W/m●k, which may be because the poor compatibility between APP particles and RPUF matrix destroyed part of the cell structure. When 30 php MFAPP was added, the density of RPUF/MFAPP30 was 54.88 kg/m$^3$, which was much lower than that of RPUF/APP30. This result indicates that much of the hydroxymethyl in MF could react with PM200, which promoted the release of $CO_2$ and thus decreased the density of the RPUF/MFAPP composite. Also, the thermal conductivity of RPUF/MFAPP30 was 0.0400 W/m●k, which was lower than that of RPUF/APP30, indicating that the MF resin enhanced the compatibility of the APP particles and RPUF matrix and inhibited the destruction of the cell structure in RPUF/MFAPP30.

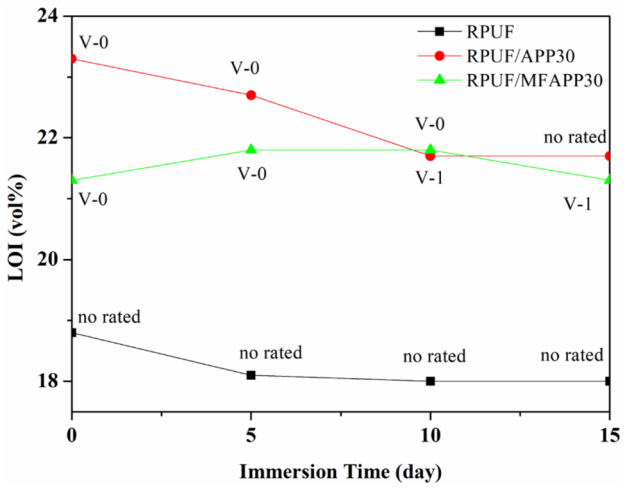


**Fig. 6** LOI and UL-94 test results for RPUF, RPUF/APP30, and RPUF/MFAPP30 with different immersion time

The compressive strength of the RPUF composites was also investigated. Virgin RPUF showed compressive strength of 0.325 MPa. With 30 php APP loaded, the compressive strength of RPUF/APP30 decreased to 0.260 MPa, which may result from the poor compatibility of the APP particles and RPUF matrix. RPUF/MFAPP30 possessed enhanced compressive strength of 0.295 MPa, which was 13.4% higher than that of RPUF/APP30, indicating enhanced interfacial compatibility between MFAPP particles and RPUF matrix [34].

## Gas phase products

TGA-FTIR is an effective method for analyzing the gas products and flame-retardant mechanism of composites [35, 36]. Figure 8 shows the 3D FTIR spectra of the volatilized products for RPUF, RPUF/APP30, and RPUF/MFAPP30. It can be seen that the characteristic degradation peaks are distributed in several regions including 3700–3800 cm$^{-1}$, 3300–3400 cm$^{-1}$, 2200–2400 cm$^{-1}$, 1400–1800 cm$^{-1}$, and 1100–1300 cm$^{-1}$ [37].

Figure 9 shows the FTIR spectra of RPUF, RPUF/APP30, and RPUF/MFAPP30 at the maximum thermal mass loss rate. The peaks at around 3730 cm$^{-1}$ corresponded to the stretching vibration of the N–H bond in urethane. The peaks at 2360 cm$^{-1}$ and 2290 cm$^{-1}$

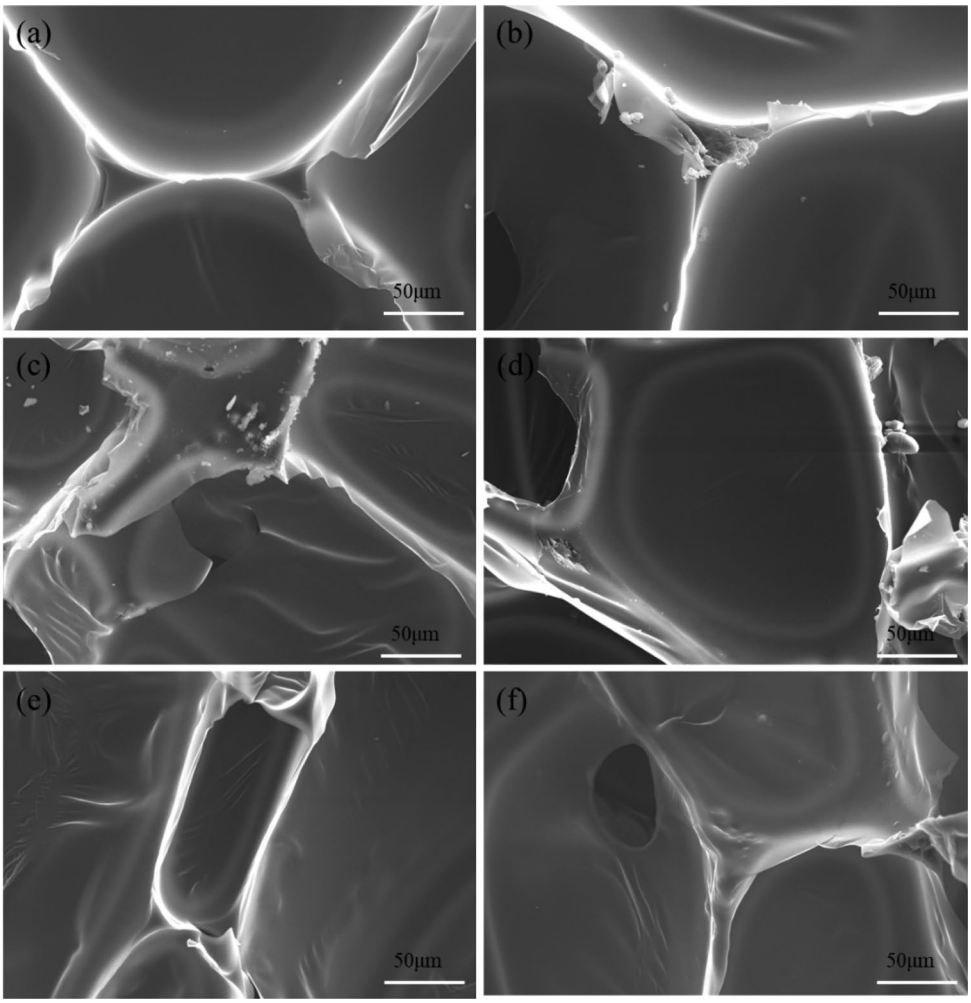


**Fig. 7** SEM images of RPUF (**a**, **b**), RPUF/APP30 (**c**, **d**), and RPUF/MFAPP30 (**e**, **f**) before immersion (**a**, **c**, **e**) and after immersion for 15 days (**b**, **d**, **f**).

confirmed the existence of $CO_2$ and isocyanate compounds, which were typical gas products of RPUF in the first stage. The peaks at around 1730 $cm^{-1}$ and 1510 $cm^{-1}$ corresponded to carbonyl compound and aromatic compound, respectively. The peaks at 1260 $cm^{-1}$ and 1110 $cm^{-1}$ can be ascribed to an ester compound [38]. The characteristic peaks of the above products were found in RPUF, RPUF/APP30, and RPUF/MFAPP30, indicating that APP and MFAPP, as additive flame retardants, did not change the pyrolysis process of the polyurethane molecular chain.

We also investigated the release of pyrolysis products of RPUF, RPUF/APP30, and RPUF/MFAPP30 versus time. It can be observed from Fig. 10 that the Gram-Schmidt curves of RPUF, RPUF/APP30, and RPUF/MFAPP30 indicate two degradation processes, which is consistent with the TGA. The first stage corresponds to the degradation of a hard segment of the polyurethane chain, and the main products were isocyanate compounds, amines, hydrocarbons, and $CO_2$ [39]. The second stage corresponded to the degradation of the soft segment, and the main product was CO. As shown in Fig. 10(b), RPUF/APP30 exhibited lower hydrocarbon intensity than virgin RPUF, which was because APP promoted more hydrocarbons into the condensed phase. Furthermore, the addition of MFAPP showed the lowest hydrocarbon intensity, implying a synergistic effect of MF and APP [40]. Figure 10(c) and (d) revealed that the intensities of $CO_2$ and the isocyanate compounds for RPUF/MFAPP30 were significantly lower than those of RPUF/APP30, which may be because the

**Table 4** Thermal conductivity, density, and compressive strength of RPUF, RPUF/APP30, and RPUF/MFAPP30

| Sample | ρ/Kg·m$^{-3}$ | λ/W·m$^{-1}$·k$^{-1}$ | Compressive strength / MPa |
|---|---|---|---|
| RPUF | 63.52 | 0.0389 | 0.325 |
| RPUF/APP30 | 64.16 | 0.0412 | 0.260 |
| RPUF/MFAPP30 | 54.88 | 0.0400 | 0.295 |

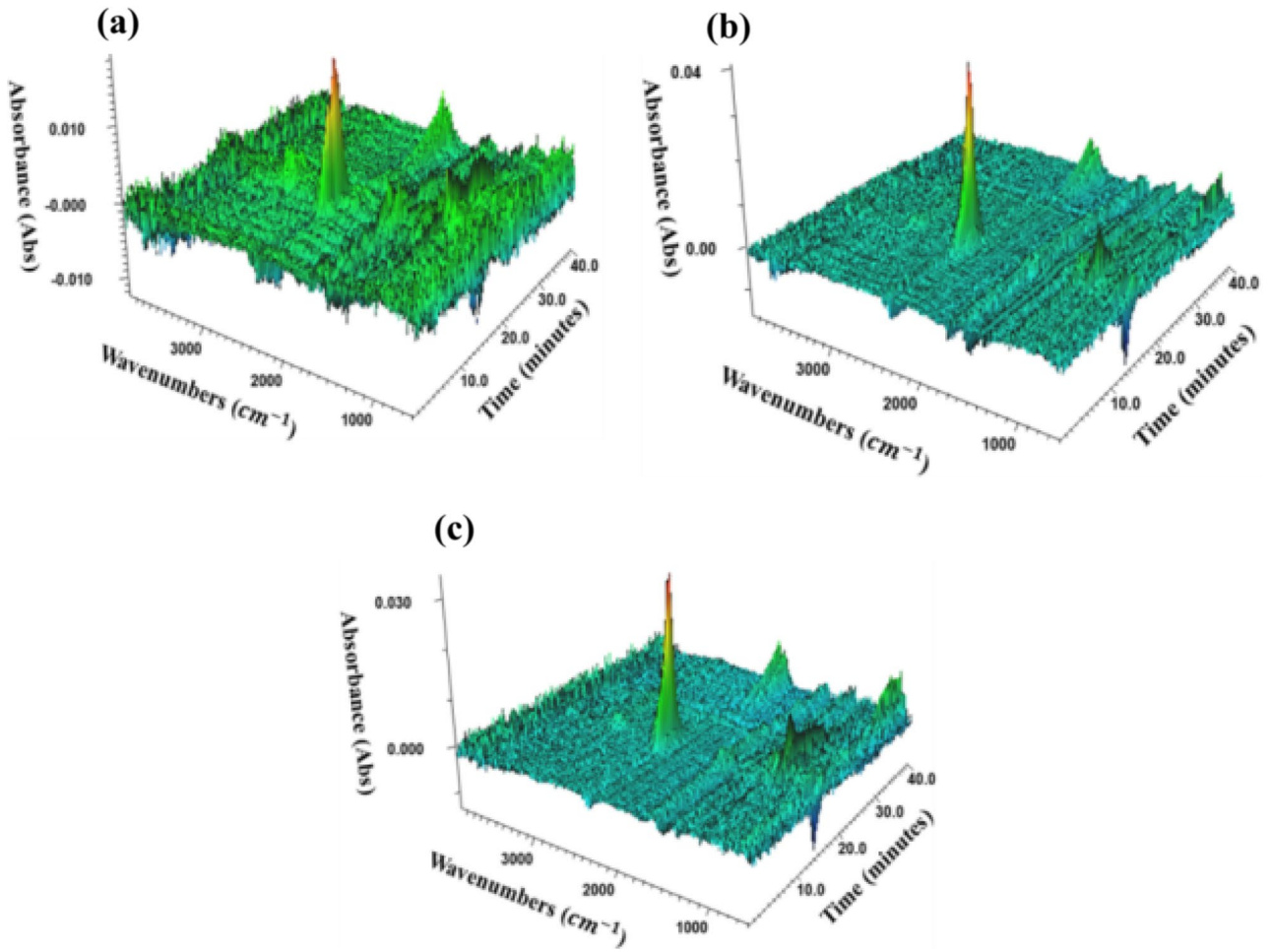


**Fig. 8** TGA-FTIR 3D spectra of RPUF (**a**), RPUF/APP30 (**b**), and RPUF/MFAPP30 (**c**)

MF shell inhibited the reaction of the APP particles and polyurethane chain. CO is a typical gaseous product of RPUF, and causes many casualties in fires [41]. It can be seen from Fig. 10(e) that the CO intensity of RPUF/MFAPP30 was lower than that of RPUF/APP30, confirming that MFAPP was safer than APP in the RPUF composites. There were two possible reasons for this. Firstly, the synergistic effect between MF resin and APP particles promoted more soft segments into the condensed phase, thus reducing the formation of CO. Secondly, the compact char residue in the combustion zone of the RPUF/MFAPP composite suppressed the release of CO outside.

## Char residue analysis

The char residues of RPUF, RPUF/APP30, and RPUF/MFAPP30 were obtained by calcining the sample at 700 °C for 10 min. Figure 11 displays the micro-morphology of the char residues for the samples. As shown in Fig. 11(a), pure

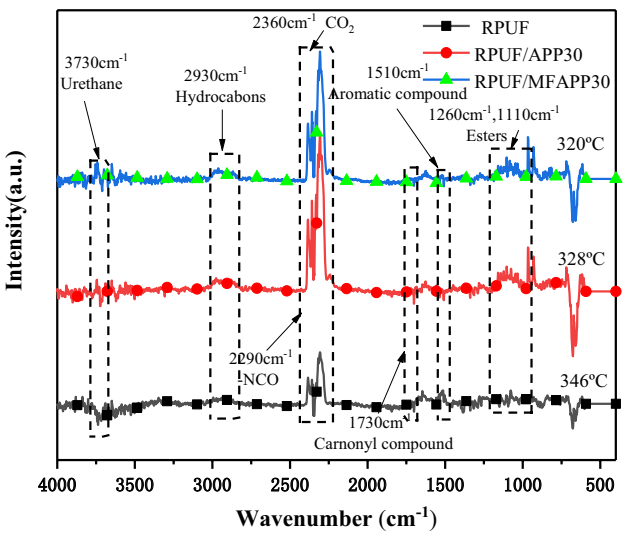


**Fig. 9** TGA-FTIR spectra of the pyrolysis products of RPUF, RPUF/APP30, and RPUF/MFAPP30 at the maximum decomposition rate

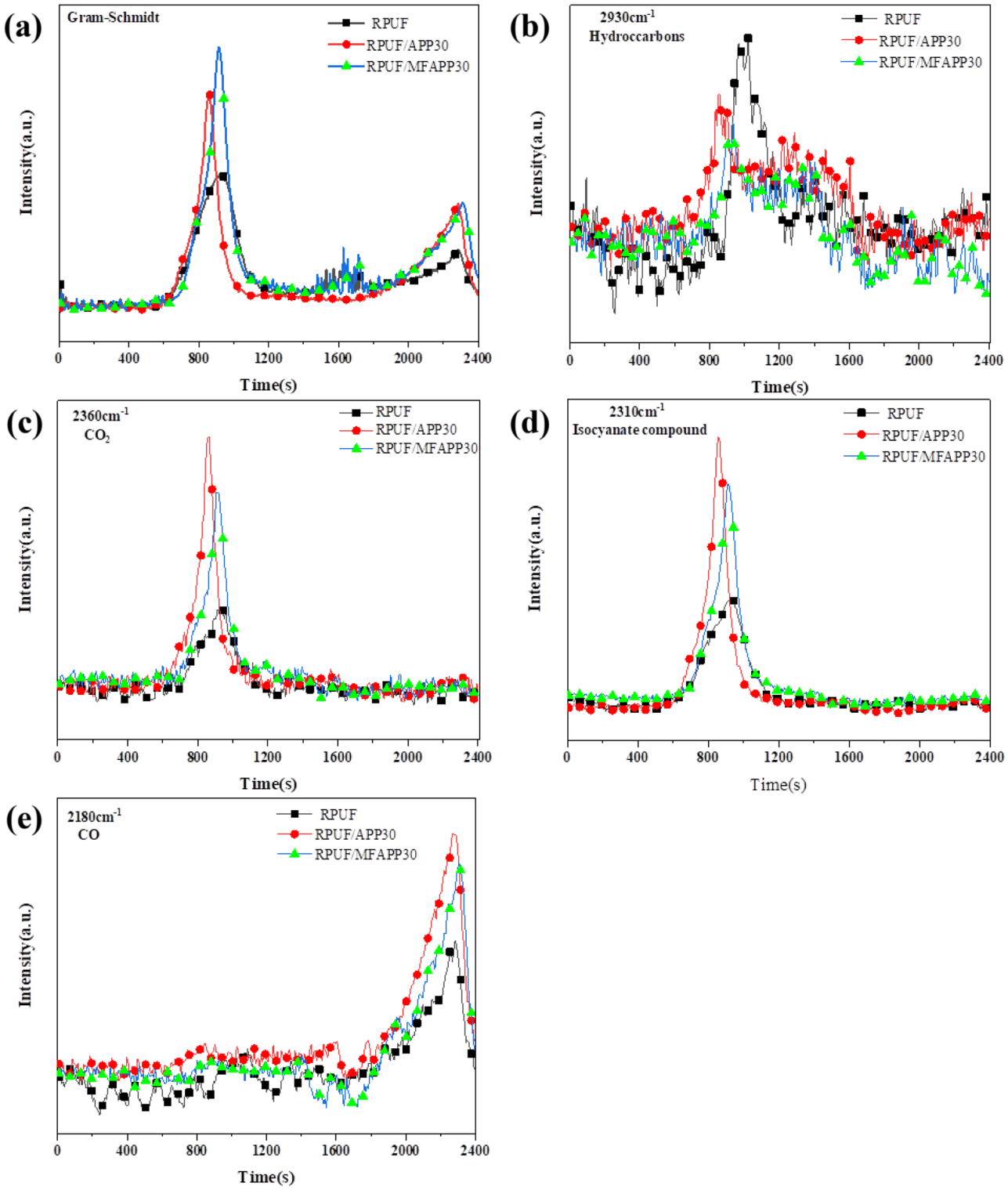


**Fig. 10** Absorbance of pyrolysis products of RPUF, RPUF/APP30, and RPUF/MFAPP30 vs. time: (**a**) Gram-Schmidt; (**b**) hydrocarbons; (**c**) $CO_2$; (**d**) isocyanate compound; (**e**) CO

RPUF showed loose residues with many holes, which were caused by the release of gas products from inside RPUF during the decomposition process. Such a structure could not inhibit the release of combustible gas and heat transmission in fire, with no flame retardancy. RPUF/APP30 demonstrated improved compactness of char residues; however,

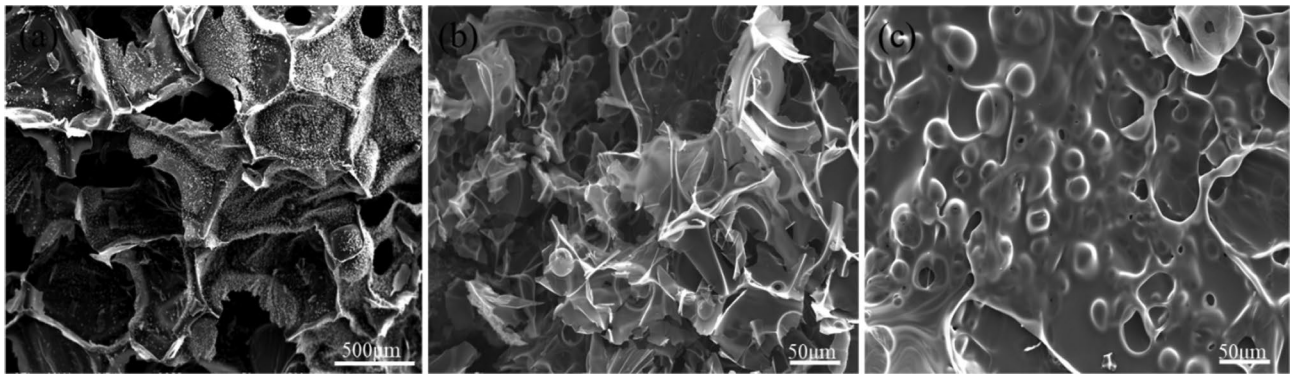


**Fig. 11** SEM images of char residues for RPUF (**a**), RPUF/APP30 (**b**), and RPUF/MFAPP30 (**c**)

a structure with a few holes was observed. As shown in Fig. 11(c), RPUF/MFAPP30 showed compact char residue with no holes, which thus served as a barrier to oxygen and combustible gases. This structure significantly inhibited mass and heat transmission, and thus effectively retarded the combustion process of the underlying materials.

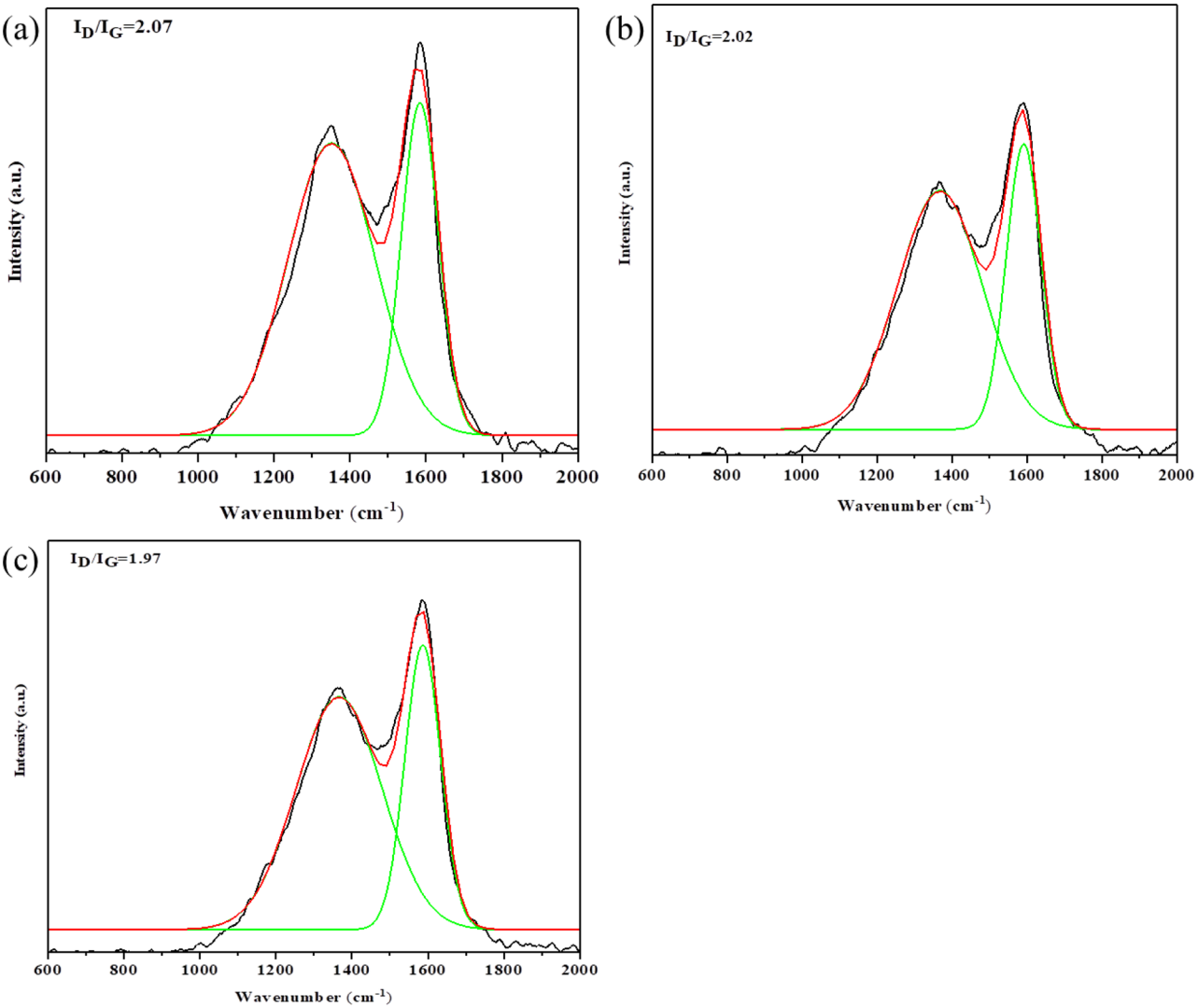


**Fig. 12** Raman spectra of char residues for RPUF (**a**), RPUF/APP30 (**b**), and RPUF/MFAPP30 (**c**)

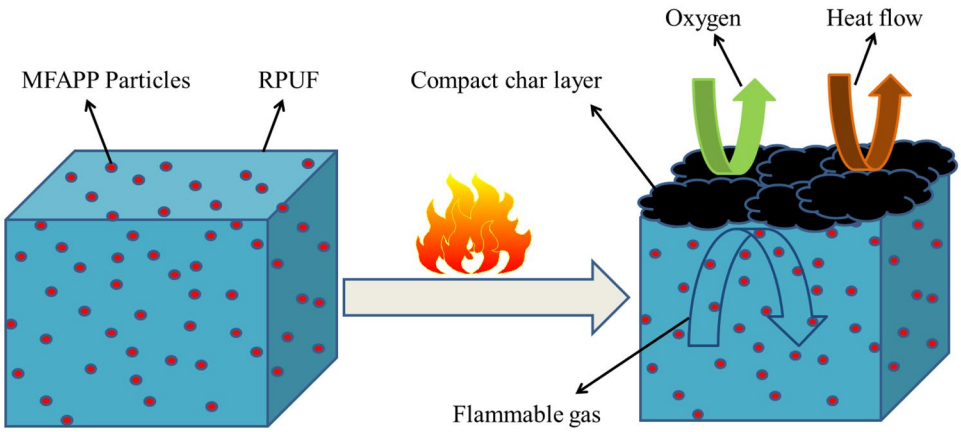


**Fig. 13** Schematic illustration for the flame-retardant mechanism of RPUF/MFAPP composites

Char quality is crucial for fire retardancy in the condensed phase. The measurement of Raman spectra is an important parameter for investigating the microstructure of materials [42, 43]. Figure 12 shows the Raman spectra of the char residues for RPUF, RPUF/APP30, and RPUF/MFAPP30. Two predominant bands are observed for the samples in the investigated wavenumber range. The band at around 1587 $cm^{-1}$ is the G band, which can be ascribed to the crystalline phase consisting of graphitic carbon atoms. The band located at 1350 $cm^{-1}$ is the D band, which corresponds to the amorphous phase consisting of disordered carbon atoms [44, 45]. The area ratio of the D and G bands ($I_D/I_G$) was determined to assess the graphitization degree of the carbonaceous materials. The $I_D/I_G$ value followed the order RPUF (2.07) > RPUF/APP30 (2.02) > RPUF/MFAPP30 (1.97). A lower $I_D/I_G$ value indicates a higher degree of graphitization and better thermal resistance for the char residues [46, 47]. As shown in Fig. 12, RPUF/MFAPP30 demonstrates a lower $I_D/I_G$ value than that of RPUF/APP30, indicating higher graphitic carbon content in the char residue of RPUF/MFAPP30, which is beneficial for thermal oxidative resistance [48].

## Consideration of Mechanism

Combined with the above data and previous literature, the possible flame-retardant mechanism of the RPUF/MFAPP composite is proposed in Fig. 13. The core material APP thermally decomposes into polyphosphoric acid (PPA) and $NH_3$. Polyphosphoric acid promotes the formation of compact char residue in the RPUF matrix, which inhibits mass and heat transmission in fire. The inflammable gas $NH_3$ can dilute combustible gases produced in the combustion process. Furthermore, the MF resin shell material is thermally decomposed into $CO_2$ and $NH_3$, which then act to dilute the flammable gases. Thus, RPUF/MFAPP achieves enhanced fire resistance properties by the gas–solid flame retardancy mechanism of MFAPP.

## Conclusions

MFAPP was fabricated by in situ polymerization and characterized by TGA, XPS, and SEM. The RPUF/MFAPP composite was prepared by a one-step water-blown method, and its flame retardancy, thermal stability, thermal conductivity, water resistance, and combustion products were investigated and compared with those of pure RPUF and RPUF/APP composite. It was found that MFAPP possessed excellent water resistance, which endowed RPUF/MFAPP with favorable flame retardancy after water immersion. TGA-FTIR revealed that RPUF/MFAPP released fewer CO and isocyanate compounds compared with RPUF/APP, implying better fire safety. SEM and Raman tests confirmed that RPUF/MFAPP presented more compact char residue with a more graphitic carbon structure, which significantly enhanced fire retardancy of the composite. All of the above characteristics imply that MFAPP is a good candidate for fabricating flame-retardant RPUF composites.

**Acknowledgements** This research was supported by the National Natural Science Fund of China (No. 51978002, No. 51403004), Open Project of State Key Laboratory Cultivation Base for Nonmetal Composites and Functional Materials (17kffk14), Provincial Natural Science Foundation of Anhui (KJ2016SD08), and Postdoctoral Science Foundation of China (2017M610399).

## References

1. Jiang T, Wang WJ, Yu DH, Huang D, Wei N, Hu Y, Huang H (2018) Synthesis and characterization of polyurethane rigid foams from polyether polyols with isosorbide as the bio-based starting agent. J Polym Res 25(6):140
2. Hoseinabadi M, Naderi M, Najafi M, Motahari S, Shokri M (2017) A study of rigid polyurethane foams: The effect of synthesized polyols and nanoporous grapheme. J Appl Polym Sci 134(26):45001
3. Yuan Y, Yu BH, Shi YQ, Ma C, Song L, Hu WZ, Hu Y (2018) Highly efficient catalysts for reducing toxic gases generation change with temperature of rigid polyurethane foam nanocomposites: A comparative investigation. Compos Part A: Appl Sci 112:142–154

4. Tang G, Liu XL, Zhou L, Zhang P, Deng D, Jiang HH (2020) Steel slag waste combined with melamine pyrophosphate as a flame retardant for rigid polyurethane foams. Adv Powder Tech 31(1):279–286
5. Wang X, Li JQ, Lin JL (2019) Flame retardant behaviour of ternary synergistic systems in rigid polyurethane foams. Polymers 11(2):207
6. Kim S, Shin H, Rhim S, Rhee KY (2019) Calibration of hyperelastic and hyperfoam constitutive models for an indentation event of rigid polyurethane foam. Compos Part B: Eng 163:297–302
7. Zhou K, Gui Z, Hu Y, Jiang SH, Tang G (2016) The influence of cobalt oxide–graphene hybrids on thermal degradation, fire hazards and mechanical properties of thermoplastic polyurethane composites. Compos Part A: Appl Sci 88:10–18
8. Yaghoubi A, Nikje MMA (2018) Silanization of multi-walled carbon nanotubes and the study of its effects on the properties of polyurethane rigid foam nanocomposites. Compos Part A: Appl Sci 109:338–344
9. Santiago-Calvo M, Blasco V, Ruiz C, París R, Villafañe F, Rodríguez-Pérez MÁ (2019) Improvement of thermal and mechanical properties by control of formulations in rigid polyurethane foams from polyols functionalized with graphene oxide. J Appl Polym Sci 136(19):47474
10. Xing WY, Yuan HX, Zhang P, Yang HY, Song L, Hu Y (2013) Functionalized lignin for halogen-free flame retardant rigid polyurethane foam: preparation, thermal stability, fire performance and mechanical properties. J Polym Res 20(9):234
11. Huang YB, Jiang SH, Liang RK, Liao ZW, You GX (2019) A green highly-effective surface flame-retardant strategy for rigid polyurethane foam: Transforming UV-cured coating into intumescent self-extinguishing layer. Compos A 125:105534
12. Huang YB, Jiang SH, Liang RK, Sun P, Hai Y, Zhang L (2020) Thermal-triggered insulating fireproof layers: A novel fire-extinguishing MXene composites coating. Chem Eng J 391:123621
13. Jiao CM, Wang HZ, Chen XL, Tang GW (2019) Flame retardant and thermal degradation properties of flame retardant thermoplastic polyurethane based on HGM@[EOOEMIm][BF4]. J Therm Anal Calorim 135(6):3141–3152
14. Wang W, Peng Y, Zammarano M, Zhang W, Li JZ (2017) Effect of ammonium polyphosphate to aluminum hydroxide mass ratio on the properties of wood-flour/polypropylene composites. Polymers 9(11):615
15. Xia Y, Jin FF, Mao ZW, Guan Y, Zheng AN (2014) Effects of ammonium polyphosphate to pentaerythritol ratio on composition and properties of carbonaceous foam deriving from intumescent flame-retardant polypropylene. Polym Degrad Stab 107:64–73
16. Luo FB, Wu K, Li YW, Zheng J, Guo HL, Lu MG (2015) Reactive flame retardant with core-shell structure and its flame retardancy in rigid polyurethane foam. J Appl Polym Sci 132(46):42800
17. Wu K, Song L, Wang ZZ, Hu Y, Kandare E, Kandola BK (2009) Preparation and characterization of core/shell-like intumescent flame retardant and its application in polypropylene. J Macromol Sci A 46(8):837–846
18. Wang W, Zhang W, Zhang SF, Li JZ (2014) Preparation and characterization of microencapsulated ammonium polyphosphate with UMF and its application in WPCs. Constr Build Mater 65:151–158
19. Ni JX, Song L, Hu Y, Zhang P, Xing WY (2009) Preparation and characterization of microencapsulated ammonium polyphosphate with polyurethane shell by in situ polymerization and its flame retardance in polyurethane. Polym Adv Technol 20(12):999–1005
20. Shen MY, Chen WJ, Kuan CF, Kuan HC, Yang JM, Chiang CL (2016) Preparation, characterization of microencapsulated ammonium polyphosphate and its flame retardancy in polyurethane composites. Mater Chem Phys 173:205–212
21. Li SX, Zhou Y, Cheng JJ, Ma QY, Zhang F, Wang Y, Liu M, Wang D, Qu WJ (2019) Mechanical property improvement and fire hazard reduction of ammonium polyphosphate microencapsulated in rigid polyurethane foam. J Appl Polym Sci 137(4):48307
22. Zheng ZH, Yan JT, Sun HM, Cheng ZQ, Li WJ, Wang HY, Zheng CXJ, Z, Yan J, Sun H, (2014) Preparation and characterization of microencapsulated ammonium polyphosphate and its synergistic flame-retarded polyurethane rigid foams with expandable graphite. Polym Int 63(1):84–92
23. Wu K, Wang ZZ, Hu Y (2008) Microencapsulated ammonium polyphosphate with urea-melamine-formaldehyde shell: preparation, characterization, and its flame retardance in polypropylene. Polym Adv Technol 19(8):1118–1125
24. Wu N, Xiu ZX, Du JY (2017) Preparation of microencapsulated aluminum hypophosphite and flame retardancy and mechanical properties of flame-retardant ABS composites. J Appl Polym Sci 134(33):45008
25. Zhu P, Gu ZJ, Shu H, Lian HL (2018) Preparation and characterization of microencapsulated LDHs with melamine-formaldehyde resin and its flame retardant application in epoxy resin. Polym Adv Technol 29(7):2147–2160
26. Liu ZT, Dai MQ, Hu QH, Liu S, Gao X, Ren F, Zhang Q (2019) Effect of microencapsulated ammonium polyphosphate on the durability and fire resistance of waterborne intumescent fire-retardant coatings. J Coat Technol Res 16(1):135–145
27. Kandelbauer A, Despres A, Pizzi A, Taudes I (2007) Testing by Fourier transform infrared species variation during melamine-urea-formaldehyde resin preparation. J Appl Polym Sci 106(4):2192–2197
28. Wang F, Zhang P, Mou YR, Kang M, Liu M, Song LX, Lu A, Rong JZ (2017) Synthesis of the polyethylene glycol solid-solid phase change materials with a functionalized graphene oxide for thermal energy storage. Polym Test 63:494–504
29. Zhou S, Lu HD, Song L, Wang ZZ, Hu Y, Ni JX, Xing WY (2009) Microencapsulated ammonium polyphosphate with polyurethane shell: application to flame retarded polypropylene/ethylene-propylene diene terpolymer blends. J Macromol Sci A 46(2):136–144
30. Sun YR, Yuan BH, Shang S, Zhang HM, Shi YQ, Yu B, Qi CR, Dong HR, Chen XF, Yang XL (2020) Surface modification of ammonium polyphosphate by supramolecular assembly for enhancing fire safety properties of polypropylene. Compos Part B: Eng 181:107588
31. Wang ZY, Han EH, Ke W (2006) Effect of nanoparticles on the improvement in fire-resistant and anti-ageing properties of flame-retardant coating. Surf Coat Tech 200(20–21):5706–5716
32. Zheng XR, Wang GJ, Xu W (2014) Roles of organically-modified montmorillonite and phosphorous flame retardant during the combustion of rigid polyurethane foam. Polym Degrad Stab 101:32–39
33. Modesti M, Lorenzetti A, Besco S, Hrelja D, Semenzato S, Bertani R, Michelin RA (2008) Synergism between flame retardant and modified layered silicate on thermal stability and fire behaviour of polyurethane nanocomposite foams. Polym Degrad Stab 93(12):2166–2171
34. Luo FB, Wu K, Lu MG, Nie SB, Li XY, Guan XX (2015) Thermal degradation and flame retardancy of microencapsulated ammonium polyphosphate in rigid polyurethane foam. J Therm Anal Calorim 120(2):1327–1335
35. Shen J, Zhang P, Song LX, Li JNP, Ji BNQ, Li JJ, Chen L (2019) Polyethylene glycol supported by phosphorylated polyvinyl alcohol/graphene aerogel as a high thermal stability phase change material. Compos Part B: Eng 179:107545
36. Zhang L, Zhang P, Wang F, Kang M, Li RQ, Mou YR, Huang YH (2016) Phase change materials based on polyethylene glycol supported by graphene-based mesoporous silica sheets. Appl Therm Eng 101:217–223

37. Tang G, Zhou L, Zhang P, Han ZQ, Chen DP, Liu XY, Zhou ZJ (2020) Effect of aluminum diethylphosphinate on flame retardant and thermal properties of rigid polyurethane foam composites. J Therm Anal Calorim 140(2):625–636
38. Yuan Y, Yu B, Shi YQ, Ma C, Song L, Hu WZ, Hu Y (2018) Highly efficient catalysts for reducing toxic gases generation change with temperature of rigid polyurethane foam nanocomposites A comparative investigation. Compos Part A Appl Sci 112:142–154
39. Yuan Y, Ma C, Shi YQ, Song L, Hu Y, Hu WZ (2018) Highly-efficient reinforcement and flame retardancy of rigid polyurethane foam with phosphorus-containing additive and nitrogen-containing compound. Mater Chem Phys 211:42–53
40. Wu K, Shen MM, Hu Y, Xing WY, Wang X (2011) Thermal degradation and intumescent flame retardation of cellulose whisker/epoxy resin composite. J Therm Anal Calorim 104(3):1083–1090
41. Wu S, Deng D, Zhou L, Zhang P, Tang G (2019) Flame retardancy and thermal degradation of rigid polyurethane foams composites based on aluminum hypophosphite. Mater Res Express 6(10):105365
42. Tang G, Liu XL, Yang YD, Chen DP, Zhang H, Zhou L, Zhang P, Jiang HH, Deng D (2020) Phosphorus-containing silane modified steel slag waste to reduce fire hazards of rigid polyurethane foams. Adv Powder Tech 31(4):1420–1430
43. Zhang H, Fang Y (2019) Temperature dependent photoluminescence of surfactant assisted electrochemically synthesized ZnSe nanostructures. J Alloys Compd 781:201–208
44. Wang SG, Gao R, Zhou KQ (2019) The influence of cerium dioxide functionalized reduced graphene oxide on reducing fire hazards of thermoplastic polyurethane nanocomposites. J Colloid Interface Sci 536:127–134
45. Shi YQ, Yu B, Zheng YY, Yang J, Duan ZP, Hu Y (2018) Design of reduced graphene oxide decorated with DOPO-phosphanomidate for enhanced fire safety of epoxy resin. J Colloid Interface Sci 521:160–171
46. Zhang JH, Kong QH, Yang LW, Wang DY (2016) Few layered $Co(OH)_2$ ultrathin nanosheet-based polyurethane nanocomposites with reduced fire hazard: from eco-friendly flame retardance to sustainable recycling. Green Chem 18:3066–3074
47. Kong QH, Sun YL, Zhang CJ, Guan HM, Zhang JH, Wang DY, Zhang F (2019) Ultrathin iron phenyl phosphonate nanosheets with appropriate thermal stability for improving fire safety in epoxy. Compos Sci Technol 182:107748
48. Zhou KQ, Tang G, Gao R, Jiang SD (2018) In situ growth of 0D silica nanospheres on 2D molybdenum disulfide nanosheets: Towards reducing fire hazards of epoxy resin. J Hazard Mater 344:1078–1089